ELSEVIER

Interpretation of large-scale structures observed in a turbulent plane Couette flow

Dimitrios V. Papavassiliou and Thomas J. Hanratty
Department of Chemical Engineering, University of Illinois, Urbana, IL

Large-flow structures, not observed in turbulent Poiseuille flow, are found in direct numerical simulations of turbulent Couette flow. Because these structures are persistent in space and time, an interpretation is presented which approximates them by a secondary flow. The asymmetry of the velocity profile is favorable to the formation of flow modules that fill the whole channel. These modules can take the form of weak rotational inviscid roll cells. They affect the turbulence in such a way that they receive energy from the turbulence, contrary to the usual notion to an energy cascade from large-scale turbulence to small-scale turbulence. *© 1997 by Elsevier Science Inc.*

Keywords: direct numerical simulation; Couette flow; turbulence; eddy structure

Introduction

Plane Couette flow in a fluid is caused by the motion of two parallel infinite planes in directions opposite to each other. It is the simplest shear field. There is no mean pressure gradient, and the driving force is a constant shear stress transmitted through the fluid from one plane to the other.

Plane Couette flow is attractive for developing theoretical models for turbulence and for hydrodynamic stability, because of the simplicity of the governing equations and the geometry (von Kármán 1937; Chandrasekhar 1961; Monin and Yaglom 1971; Drazin and Reid 1981). Reports of laboratory investigations, however, are scarce, because technical difficulties are encountered in constructing an experimental system. The moving plane is usually a belt or a fluid interface, (Reichardt 1956; Robertson 1959; Robertson and Johnson 1970; Leutheusser and Chu 1971; Aydin and Leutheusser 1979, 1991; El Telbany and Reynolds 1980, 1982), which deforms at high-Reynolds number. Measurements of mean velocity, turbulence intensities, turbulent shear stress, and skin-friction coefficient have been reported.

Direct numerical simulations (DNS) at low-Reynolds numbers have been exploited in several recent investigations to obtain more information about this flow field (Miyake et al. 1987; Lundbladh and Johansson 1991; Lee and Kim 1991; Papavassiliou 1993; Bech et al. 1993; Bech and Andersson 1994; Komminaho *et al.* 1996). A common feature of these studies of turbulent Couette flow is the observation in the xz-plane of streaks of high and low streamwise velocity in the central region of the channel, that are characterized by scales of the streamwise velocity fluctuations in the flow direction that are much larger than those found in turbulent Poiseuille flow. In this paper, these are differentiated from the well-known structures in the viscous wall region by the use of the term "wall streaks." Lundbladh and Johansson determined the critical Reynolds number, defined using one-half the distance between the planes and one-half the velocity difference. They studied a range of Re between 300 and 1500 and found that turbulence can be sustained for Re above 375. A direct numerical simulation with a coarse grid at Re = 750–1750 by Miyake et al. showed a spanwise variation of the correlation coefficient for the streamwise velocity fluctuations that suggests periodic structures. Lee and Kim presented results on the mean velocity, second-order velocity statistics, and the structure of turbulence. A $128 \times 129 \times 192$ (x, y, z) grid in a $4\pi h \times 2h \times (8/3)\pi h$ computational box was used, where $h = 170$ is the half-channel height in the wall units. Their results suggest that the streaks are associated with elongated roll cells. The cells fill the entire channel and contribute about 30% to the total turbulent kinetic energy. Bech et al. used a $96 \times 64 \times 64$ grid in a $4\pi h \times 2h \times 2\pi h$ box, where $h = 85$ wall units. As did Lee and Kim, they observed the large-scale structures in the outer region of the flow. The effect of computational box size was investigated by Bech and Andersson. They found that an increase of the length of the box by a factor of 4 ($384 \times 64 \times 64$ grid points in a $16\pi h \times 2h \times 2\pi h$ box) made the large-scale structures more distinct; an increase of the width of the channel by a factor of 2 showed large-scale structures that meander in the flow field. Laboratory measurements of the correlation coefficient of the streamwise velocity fluctuations at Re = 1300 by Bech et al. (1995) show a spanwise variation, which is consistent with the computer simulations.

The present paper uses a simulation at Re = 2660 to examine the structures discovered by Lee and Kim (1991). Our viewpoint is that these can be treated as secondary flows, because they persist in both space and in time. Over most of the flow field, the secondary flow is found to be described by the equations for an inviscid rotational field; viscous and turbulent stresses are important close to the boundaries.

Bradshaw (1987) distinguished two types of turbulent secondary flows. One, Prandtl's first kind, is generated by a redirec-

Address reprint requests to Dr. Thomas J. Hanratty, Department of Chemical Engineering, University of Illinois, Urbana, IL 61801, USA.

Received 10 March 1996; accepted 15 October 1996

Int. J. Heat and Fluid Flow 18: 55–69, 1997

655 Avenue of the Americas, New York, NY 10010

0142-727X/97/$17.00
PII S0142-727X(96)00138-0

tion or skewing of spanwise vorticity to the streamwise direction. This vorticity is later diffused by Reynolds and viscous stresses. The other, Prandtl's second kind of secondary flow, occurs when streamwise mean vorticity is generated by Reynolds stresses. This is the case in rectangular ducts with boundaries in the spanwise direction. A particular concern of this paper is to determine how a secondary flow could be sustained in a channel without corners. A consideration of the energy balance equations shows that secondary flows can exist in stationary turbulence if the small rate of dissipation, due to viscosity, is balanced with energy supplied by the turbulence. This interpretation is supported by calculating the Reynolds stresses with velocity data generated by the simulation. This result is of particular interest, because turbulence usually receives energy from the mean flow. The transfer energy from the turbulence implies a negative eddy-viscosity, which can be considered as a consequence of the fact that a turbulent stress component σ_{ij} is related to all components of the rate of strain tensor and not just to $\overline{D_{ij}}$, for flows in which the average velocity is three-dimensional (3-D).

Numerical procedures

The computer code used in this work is a modification of an algorithm developed by McLaughlin (see Lyons et al. 1991 and a thesis by Lyons 1989), which simulates fully developed turbulent flow in a channel. The fluid is Newtonian and incompressible, and it has constant physical properties.

The simulation is carried out on a $128 \times 65 \times 128$ grid in x, y, and z. The streamwise direction is x, the spanwise is z, and the direction perpendicular to the channel walls is y. The dimensions of the computational box are $4\pi h \times 2h \times 2\pi h$, where h is the half-height of the channel. The flow is regarded as periodic in the streamwise and spanwise directions, with periodicity lengths equal to the size of the computational box in these directions. No-slip boundary conditions are imposed at the rigid channel walls. The Navier–Stokes equations are integrated in time using the pseudospectral fractional step method developed by Orszag and Kells (1980) with a pressure field correction suggested by Marcus (1984). The velocity field is expanded in truncated Fourier series in the x-direction, the z-direction, and a truncated Chebyshev polynomial series in the normal direction. The velocity field advances from time N to time $N+1$ by three fractional steps. In the first fractional step, the nonlinear convective term is calculated. The second fractional step calculates the dynamic pressure head, and the third fractional step solves for the viscous terms. The convective term is advanced in time by a second-order accurate semi-implicit Adams–Bashforth–Crank–Nicholson scheme; the largest contribution to the convection term $\bar{U}(\partial U/\partial x)$ is treated implicitly using a Crank–Nicholson scheme, and the rest of the convective term is treated explicitly with an Adams–Bashforth scheme. The dynamic pressure term and the viscous term are advanced in time by a first-order accurate Euler scheme. The convective (nonlinear) term is evaluated in physical space and, thus, aliasing errors occur, which are reduced by using the two-thirds truncation rule.

For the simulation of turbulent flow in a channel, it is convenient to use the wall variables, the kinematic viscosity ν, and the friction velocity u^*, to make the equations nondimensional. For plane channel flow, the Reynolds number is introduced through the mean pressure gradient. In Couette flow, however, there is no mean pressure gradient, so the Reynolds number is introduced in a different way. The equations for Couette flow were made nondimensional, so that the half channel height was $h = 150$, and the size of the computational box was $1900 \times 300 \times 950$. The time-step used was 0.2 time units. The normalizing factors were different from the calculations for Poiseuille flow by a constant factor.

In Couette flow, the walls are moving relative to each other. This is taken into account by changing the Dirichlet boundary conditions. For plane channel flow, the velocity vector is set to zero at the walls, while for Couette flow the streamwise velocity

Notation

A, B	constants in log-law relation
C	streamfunction amplitude
D	rate of strain tensor
$\frac{D}{Dt}$	substantial derivative
G	constant defined as $U_w = \pm Gh$
h	half-channel height
k_x	wavenumber in the streamwise direction
N	time iteration
$\overline{P}$	ensemble average of the pressure
p	pressure fluctuation
p^s	secondary pressure
q^2	two times the turbulent kinetic energy
Re	Reynolds number $= \frac{U_w h}{\nu}$
Re_c	critical Reynolds number $= \frac{U_w h}{\nu}$
t	time
u^*	friction velocity $= \left(\frac{\tau_w}{\rho}\right)^{1/2}$
U_w	streamwise velocity of the walls of the Couette flow channel
$\overline{U_i}$	ensemble average of the ith component of the velocity
u, v, w	fluctuating velocity components in the x-, y-, z-directions
u^s, v^s, w^s	secondary velocity components in the x, y, z directions
x, y, z	streamwise, normal, and spanwise coordinates

Greek

α_i	wavenumber in the ith direction
ϵ	eddy-viscosity
ϵ_{ijk}	permutation index
λ^+	streak spacing in the wall region
λ_i	wavelength in the ith direction
ν	kinematic viscosity
σ	turbulent stress tensor
τ_w	shear stress at the wall
ψ	streamfunction
ω_i	vorticity component in the ith direction

Superscripts and subscripts

$\overline{(\ )}$	ensemble average
$\langle\ \rangle$	average over the x, z directions and time
$(\ )^s$	value associated with the secondary flow
$(\ )^+$	value made dimensionless with the wall parameters
$(\ )_w$	value at the wall

at the wall U_w is given by

$$U_w = \pm Gh \tag{1}$$

where G is a constant ($G = 0.11826$), which specifies the Reynolds number of the simulated field. The choice of G is such that the dimensionless variables calculated in the code have values as close as possible to their values in wall units. The top wall of the channel moves in the minus x-direction, and the bottom wall moves in the positive x-direction. The Reynolds number Re, defined as $\mathrm{Re} = (U_w h/\bar{v})$, is 2660; this is much higher than the critical value for plane Couette flow. The experiments of Reichardt (1956) give $\mathrm{Re}_c = 750$. The more recent studies by Aydin and Leutheusser (1991) and by Tillmark and Alfredsson (1992) report values of 300 and 360 ± 10, respectively.

The code was run in two stages. The initial trial stage was on a coarse grid ($16 \times 33 \times 64$). When a stationary state was successfully reached, the runs for the second stage were started on a fine grid.

The initial velocity field, which was used to start the simulation, was a Poiseuille flow velocity field at stationary state. The top half of the profile was selected to be a turbulent Poiseuille flow and the bottom half, the mirror image of the top. This profile gives a velocity at the bottom of the channel equal to the maximum of the turbulent Poiseuille mean velocity. The fluctuating velocity field adjusted to this mean velocity profile in about 100 time units for both the coarse and the fine grids. After 2000 time units, the flow field reached a stationary state that was identified when both the second-order statistics of the flow and the mean kinetic energy balance converged. The simulation was continued for another 2250 time units to acquire meaningful statistics of the flow. The characteristic velocity was found to be $1.04748u^*$ in the intrinsic units chosen for the simulation. Thus, the half-channel height in wall units is $h^+ = 157$.

The coarse grid simulation and the transient state of the fine grid simulation were run on one processor of a CRAY-2 supercomputer up to 10,000 time-steps; the latter required about 150 CPU hours. The stationary state results were acquired on one processor of a CONVEX C3880 supercomputer and required about 220 CPU hours for 11250 time iterations.

The resolution of the calculations presented in this paper is the same as used in previous studies of turbulent flow in a channel (Lyons et al. 1991). The numerical accuracy of these simulations was verified by a comparison with laboratory measurements at the same conditions (Niederschulte 1989).

Results

Velocity measurements

Mean velocities are plotted in Figure 1 in semilogarithmic coordinates. The abscissa is the distance from the wall made dimensionless with wall coordinates. The ordinate is the absolute value of the difference between the velocities of the wall and the fluid. The velocity profile is asymmetric about the centerline of the channel; only one half of this profile is shown. A logarithmic relation extends from $y^+ = 40$ to $y^+ = 260$, a distance of about 220 wall units. It is described by the relation

$$\overline{U^+} = 2.30 \ln y^+ + 5.25 \tag{2}$$

Lee and Kim (1991) obtained values of 2.31 and 5.8 for the constants in the above equation. Results from different investigations are summarized in Table 1.

Calculated values of the dimensionless root-mean-square of the three components of the velocity fluctuations are presented as the solid curves in Figure 2. The calculations of Lee and Kim (1991) are represented by the dashed curves. The datapoints are laboratory measurements. Good agreement is observed with measurements and with the calculations of Lee and Kim. Calculations of the Reynolds stress and the total stress are presented in Figure 3.

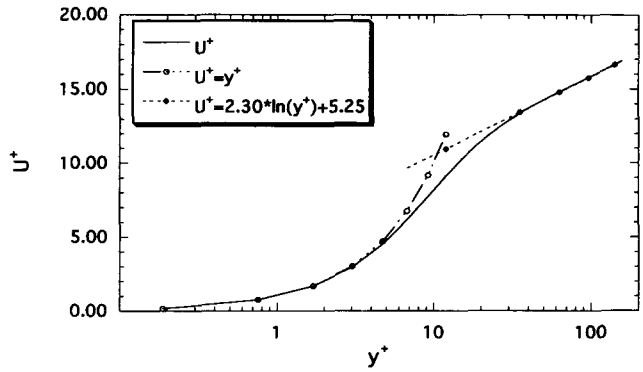

Figure 1 Mean velocity profile in wall units

The kinetic energy of the turbulence per unit mass is given as $\overline{q^2}/2$, where $\overline{q^2} = \overline{u_i^2}$. The energy balance is given by Hinze (1987) as

$$-\overline{uv}\frac{dU}{dy} - \frac{\partial}{\partial y}\left(\frac{1}{2}\overline{q^2 v}\right) - \frac{\partial \overline{pv}}{\partial y^2} + \frac{\partial^2}{\partial y^2}\left(\frac{1}{2}\overline{q^2}\right) - \overline{\left(\frac{\partial u_i}{\partial x_j}\right)^2} = 0 \tag{3}$$

where all terms have been made dimensionless with the friction velocity and the kinematic viscosity. The first term represents the production; the second, the transport by turbulence; the third, the work done by pressure fluctuations; and the fourth, the viscous diffusion. The last term, the dissipation of turbulent energy, is strictly applicable to a homogeneous field. A complete consideration of both homogeneous and nonhomogeneous terms in the exact formulation of the energy dissipation shows that the error involved in using Equation 3 is negligible (Papavassiliou 1993). A plot of the terms in Equation 3 is given in Figure 4. There is is a slight net transfer of energy from the inner flow to the log-layer due to the turbulent transport and the pressure work. However, the production and dissipation are roughly equal to one another in the log-layer.

The spatial correlation coefficients of the three velocity components at the center of the channel, in the direction of the flow, are shown in Figure 5. As has already been noted, the length scale of the streamwise velocity fluctuations in the streamwise direction is much larger than what is observed in turbulent Poiseuille flow. Correlation coefficients, at the center of the channel, in the spanwise direction are given in Figure 6. A

Table 1 Reported values for the logarithmic law constants ($U^+ = A \ln y^+ + B$)

Investigator	A	B
Reichardt (1956)	2.48	5.5
Leutheusser and Chu (1971)	2.49	6.0
Robertson and Johnson (1970)	2.43	5.6
El Telbany and Reynolds (1982)	2.55	5.2
Aydin and Leutheusser (1991)	2.5	5.5
Lee and Kim (1991)	2.31	5.8
Present work	2.30	5.25

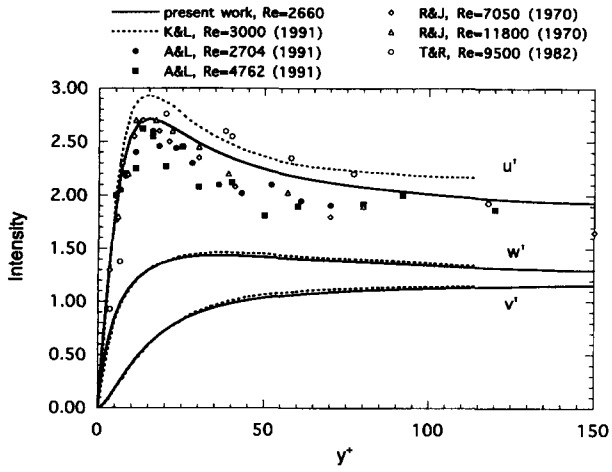

Figure 2 Intensity profiles for plane Couette flow in wall units; L & K, Lee and Kim (1991); A & L, Aydin and Leutheusser (1979; 1991); R&J, Robertson and Johnson (1970); T&R, El Telbany and Reynolds (1980; 1982)

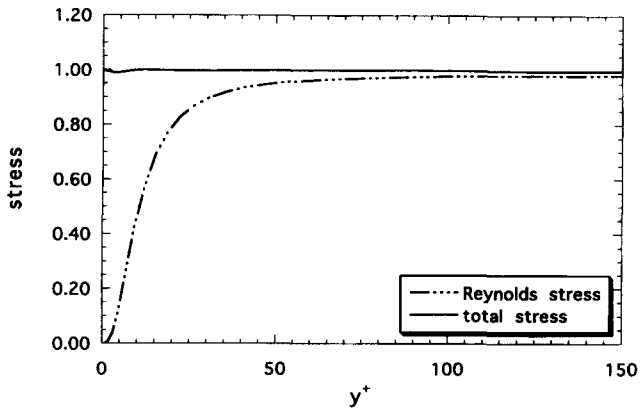

Figure 3 Profile of total stress and Reynolds stress for plane Couette flow in wall units

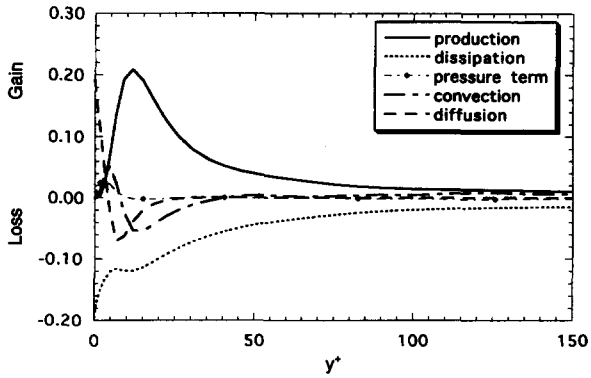

Figure 4 Turbulent kinetic energy budget

periodicity is noted for the streamwise and normal components.

Flow patterns

Figure 7a is a typical instantaneous velocity field in a cross section perpendicular to the direction of the mean flow, at $x = 29.7$. The arrows represent the projection of the fluctuating velocity vectors on the plane. The velocity scale is presented in

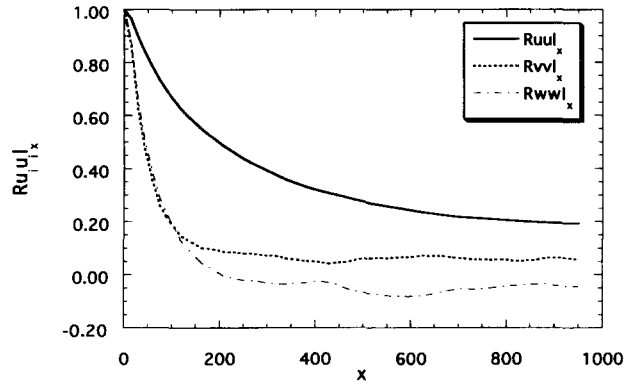

Figure 5 Two-point correlation coefficient with streamwise separation at the center of the channel

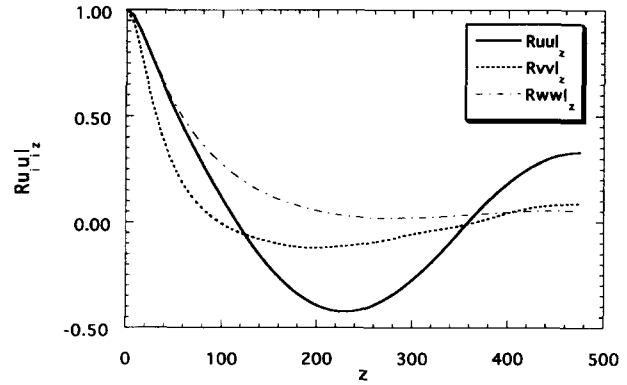

Figure 6 Two-point correlation coefficient with spanwise separation at the center of the channel

the upper right corner of the figure. The dimensions of the figure are in simulation units; the results can be converted to wall units by a multiplication with $u^*/\nu = 1.04748$. The bottom wall is moving from the reader to the paper plane; the top wall is moving in the opposite direction. Eddies exist not only in the region close to the wall but also in the center region. Roll cells cannot be identified in this single realization. However, if all vectors with positive velocities in the y-direction are plotted (as in Figure 7b) flow structures which fill the whole channel are observed. Figure 8a is a top view of a plane at the center of the channel.

The same velocity field realization is used for both Figure 7 and Figure 8. Only the positive streamwise velocity fluctuations are presented, so the blank portions of the figure correspond to regions where the streamwise velocity fluctuations are negative. These are two positive streamwise velocity streaks in Figure 8, extending from one end of the channel to the other. The streaks are not perfectly straight, but they are not interrupted all the way through the channel, even though there are regions in the streaks where the streamwise component of the velocity is small compared to the spanwise component. After a stationary state is reached, these streaks show up at the same spanwise location in the xz-plane at the center of the channel for all times studied. Figure 8c shows vectors with positive velocity components in the normal direction; the streaky structure is not so evident. As would be expected, no streamwise streaks are evident in a plot of positive spanwise fluctuations at the center of the channel (Figure 8b).

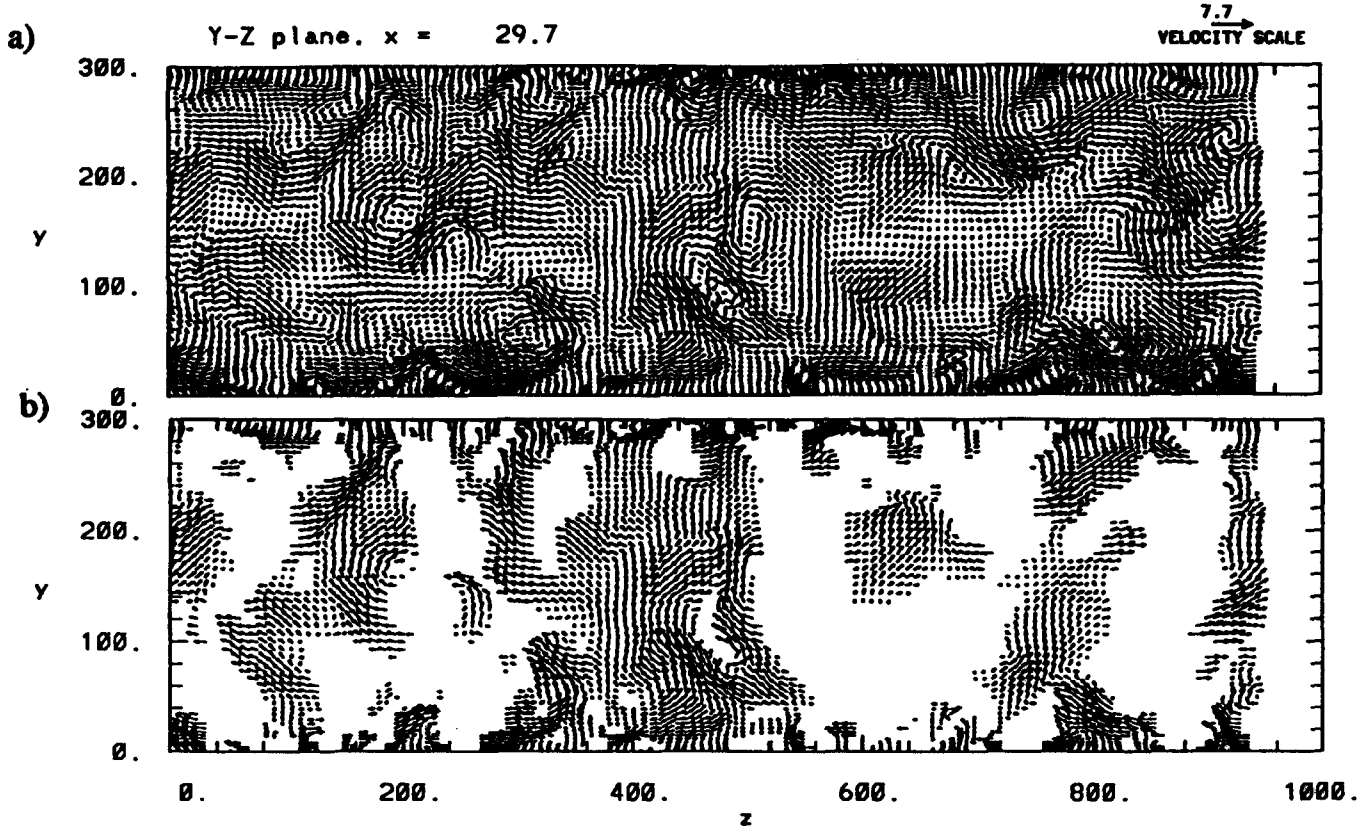

Figure 7 a) Typical *yz*-plane of Couette flow at stationary state; b) v > 0 fluctuations only

To reveal the persistent structure in the *yz*-plane, averages in the streamwise direction, over the whole channel length, were obtained. Figure 9 presents the average of results from 17 realizations of the velocity flow field, covering a time span of 2150 time units. The small-scale structures close to the wall are filtered out in the averaging; the pattern that survives is a set of roll cells that fill the entire channel and have a spanwise width of about 250 wall units. The locations of these rolls were the same for averages over time intervals of 2100–3400 and 3400–4250. These flow structures are equivalent to the $k_x = 0$ mode identified by Lee and Kim (1991). Figure 10a and 10b show the conditionally averaged velocity fields for a Couette flow and for a Poiseuille flow (in the *yz*-plane) with the condition of large positive streamwise velocities at $y = 150$ and $z = 950$. The trigger level is selected so as to capture 50% of the measured $\overline{u^2}$. The cellular structure seen in the Couette flow is not evident in the Poiseuille flow, which uses a velocity scale which is 2/7 of that characterizing Figure 9b.

Figure 11 shows velocity fields that are conditionally averaged so as to capture 60% of the Reynolds stress contributed by second quadrant events for the Poiseuille flow and by first quadrant events for a Couette flow at $y = 11.4$. A well-defined, conditionally averaged cell with a width of about 50 wall units is obtained for the Poiseuille flow (Figure 11a). This is consistent with the observation in a number of previous investigations that vortices of this size are controlling turbulence production in the viscous wall region. The velocity field for a Couette flow (Figure 11b), seems to result from a combination of the roll cells shown in Figure 9a and wall vortices with a size of about 50 wall units.

Lee and Kim (1991) reported that the large-scale structures existed even when the length of the computational box was $1024h\pi$. They suggested that the box should be longer than the viscous wall region streaks (about 1000 wall units), and the spanwise extent should include two pairs of roll-cells. It should be noted that Lee and Kim used an initial velocity profile different from that used in the present study and a spatial resolution about two times finer. They started their simulation with a linear mean velocity profile with imposed finite amplitude random disturbances. Lee and Kim report that the amount of kinetic energy associated with the $k_x = 0$ mode is about 30% of the total turbulent kinetic energy; this is about 25% for the present simulation.

Approximation of large structures by a secondary flow

The results shown in Figures 7–11 suggest that it might be useful to consider that the streaks in the mean velocity at the center of the channel are associated with a secondary flow that is part of the mean velocity vector. The total velocity vector **U** can be decomposed as

$$\mathbf{U} = \overline{\mathbf{U}} + \mathbf{u} \tag{4}$$

where $\overline{\mathbf{U}}$ is the ensemble average of the velocity, and **u** is the fluctuation. The components of the ensemble average velocity vector are

$$\overline{\mathbf{U}} = \left(\overline{U}_x, \overline{U}_y, \overline{U}_z\right) = (\langle U \rangle + u^s, v^s, w^s) \tag{5}$$

where $\langle U \rangle$ is the average velocity over the x, z-directions and time, and the superscript s denotes velocity components associ-

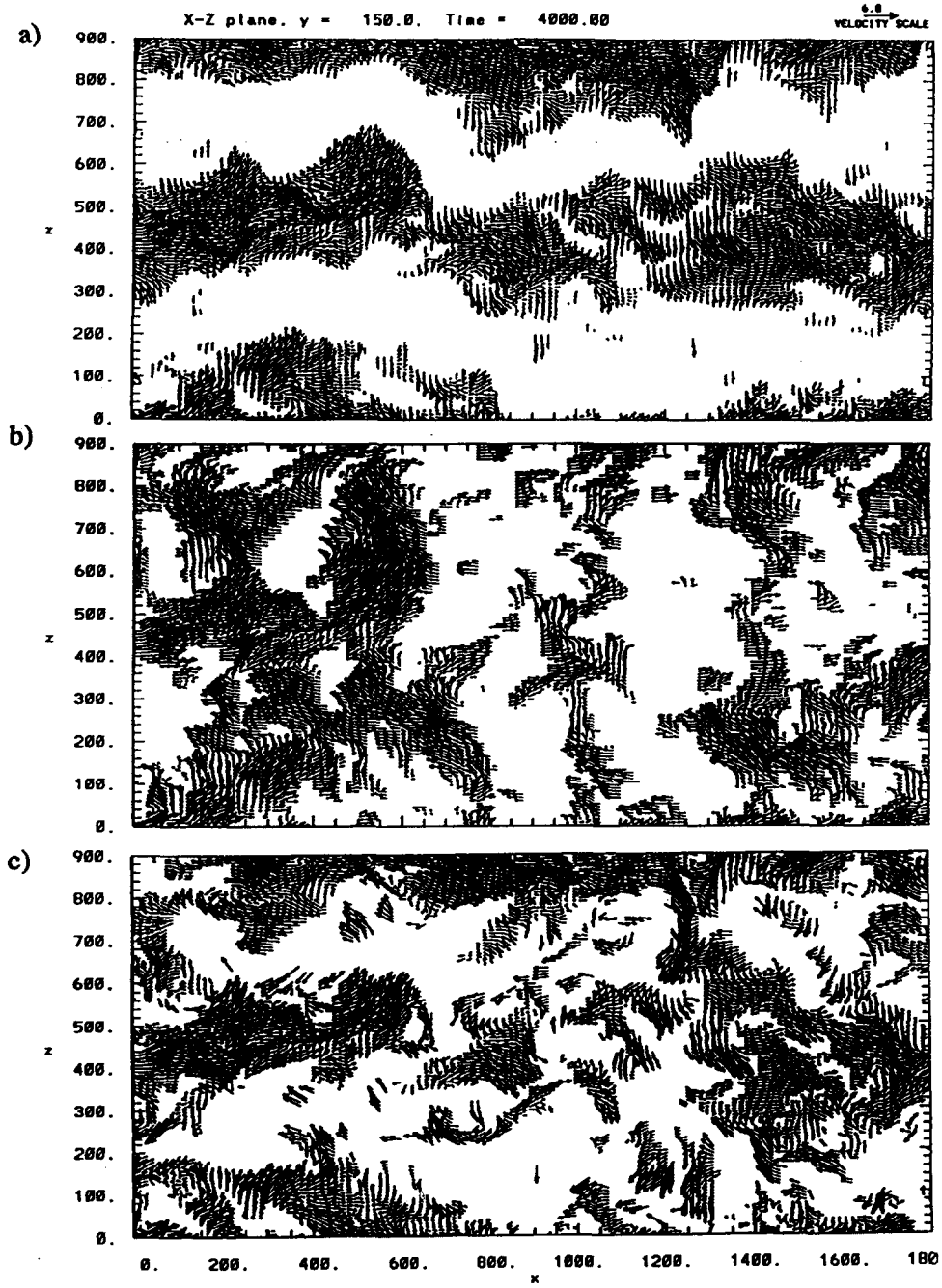

Figure 8 Instantaneous events in the *xz*-plane at the center of the channel; a) positive streamwise velocity fluctuation events; b) positive spanwise velocity fluctuation events; c) positive normal velocity fluctuation events

ated with the secondary flow. Component $\langle U \rangle$ is a function of the distance from the wall y, while u^s, v^s, and w^s are functions of both y and z.

The above approach is reasonable, because the roll cells were found to be persistent both in time and in space. The convection velocity of the large-scale structures at the center region of the channel is found to be zero (Papavassiliou 1993), which indicates that the roll cells are stationary and are not convected downstream. Furthermore, as shown in Figure 12, the viscous wall region of the Couette flow exhibits well defined $\lambda^+ = 100$ wall streaks only when the velocity fluctuations are defined as in Equation 4.

For the experiments reported in this paper, u^s, v^s, and w^s were obtained by averaging over the length of the channel for 17 realizations of the velocity field. Figure 13 presents the spanwise average of the root-mean-square values of the secondary flow velocity components. Figure 14 presents the spanwise average of the intensities of the velocity fluctuations. The secondary flow is weaker than the turbulence, as is suggested by the smaller scale for the vectors in Figure 9a than for the vectors in Figure 7a. The

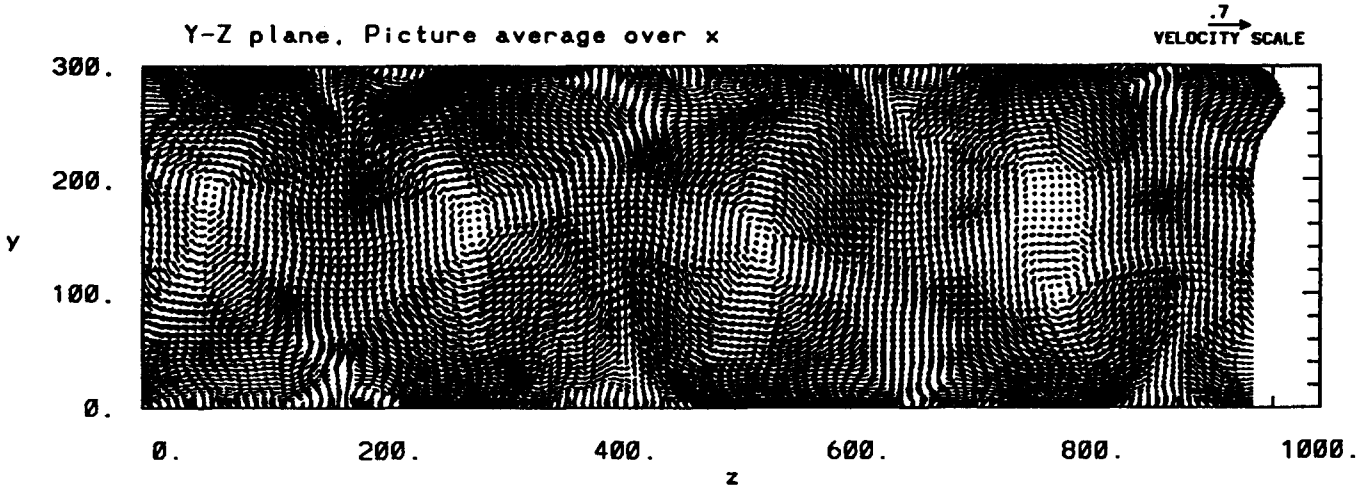

Figure 9 Streamwise average of 17 realizations of plane Couette flow velocity fields

rms of the normal component of the secondary flow velocity is about 35% of the corresponding normal turbulent velocity component at the center of the channel; it becomes much smaller closer to the wall. The rms of w^s is about 25% of the rms of w in the region close to the wall and about 5% of the rms of w at the center of the channel. The rms of u^s is about 70% of that for u at the center region of the channel. Because u^s and v^s are persistent and in phase, the rather weak secondary flow makes a large contributions to the transfer of x-momentum in the channel. Figure 15 shows the relative contribution of the secondary flow, expressed as $\langle u^s, v^s \rangle$, and of turbulence, expressed as the Reynolds stress, to the total convective transport of x-momentum, which is $\langle (u^s + u)(v^s + v) \rangle$. The brackets indicate averages in x, z, and time. In the core region of the channel, the secondary flow contributes about 40% of the total convective transport of x-momentum.

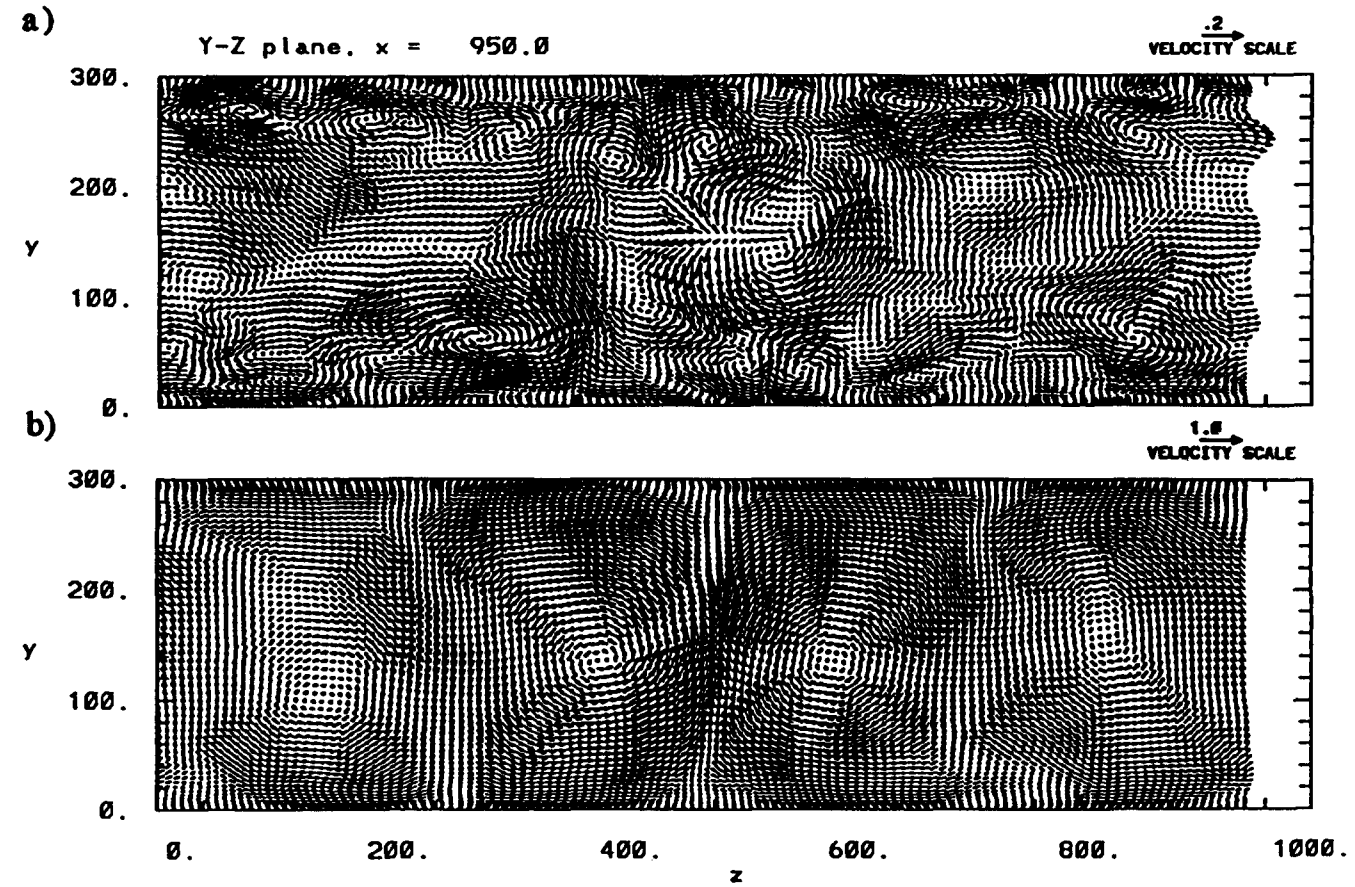

Figure 10 yz-plane of conditionally averaged velocity field with 50% of $u > 0$ events at the center of the channel; a) Poiseuille flow; b) Couette flow

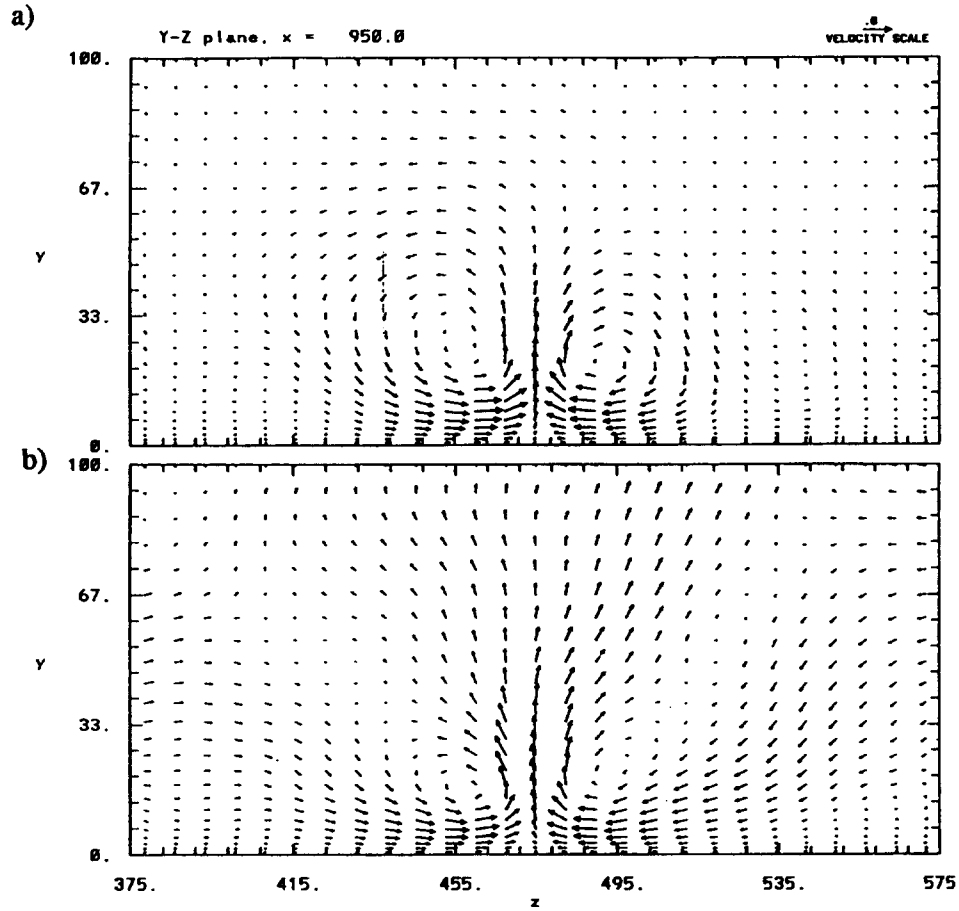

Figure 11 *yz*-plane of conditionally averaged velocity field with 60% of Reynolds stress events at $y=11.4$; a) second quadrant events in Poiseuille flow; b) first quadrant events in Couette flow

Description of the secondary flow

Governing equations

The momentum equation and the continuity equation for the ensemble average velocity at stationary state are given in wall units by (Hinze 1987)

$$\overline{U}_j\frac{\partial\overline{U}_i}{\partial x_j}=-\frac{\partial\overline{P}}{\partial x_i}+\frac{\partial^2\overline{U}_i}{\partial x_j^2}-\frac{\partial\overline{u_iu_j}}{\partial x_j} \tag{6}$$

$$\frac{\partial\overline{U}_i}{\partial x_i}=0 \tag{7}$$

where $\overline{P}$ is the ensemble average of the pressure, and the summation convention is applied. Velocity component $\overline{U}_i$ is considered to be the sum of an average value in the x, z-directions and a secondary flow component (Equation 5). Note now that the continuity equation gives

$$\frac{\partial v^s}{\partial y}+\frac{\partial w^s}{\partial z}=0 \tag{8}$$

because $\partial\overline{U}_x/\partial x=0$. Thus a streamfunction ψ associated with the secondary flow can be defined as

$$v^s=\frac{\partial\psi}{\partial z},\qquad w^s=-\frac{\partial\psi}{\partial y} \tag{9}$$

The kinetic energy equation for the mean flow is obtained by multiplying Equation 6 by $\overline{U}_i$:

$$\frac{1}{2}\frac{\partial\overline{U}_i^2\overline{U}_j}{\partial x_j}+\frac{\partial\overline{U}_i\overline{u_iu_j}}{\partial x_j}-\overline{u_iu_j}\frac{\partial\overline{U}_i}{\partial x_j}=-\overline{U}_i\frac{\partial\overline{P}}{\partial x_i}+\frac{\partial}{\partial x_j}\overline{U}_i\left(\frac{\partial\overline{U}_i}{\partial x_j}+\frac{\partial\overline{U}_j}{\partial x_i}\right)-\frac{\partial\overline{U}_i}{\partial x_j}\left(\frac{\partial\overline{U}_i}{\partial x_j}+\frac{\partial\overline{U}_j}{\partial x_i}\right) \tag{10}$$

where, again, all variables are made dimensionless with wall parameters.

The mean vorticity transport equation can be obtained by taking the curl of Equation 6. The resulting equation for the stationary state is (Speziale 1982)

$$\overline{U}_j\frac{\partial\overline{\omega}_i}{\partial x_j}=\overline{\omega}_j\frac{\partial\overline{U}_i}{\partial x_j}-\varepsilon_{ijk}\frac{\partial^2\overline{u_mu_k}}{\partial x_j\,\partial x_m}+\frac{\partial^2\overline{\omega}_i}{\partial x_j^2} \tag{11}$$

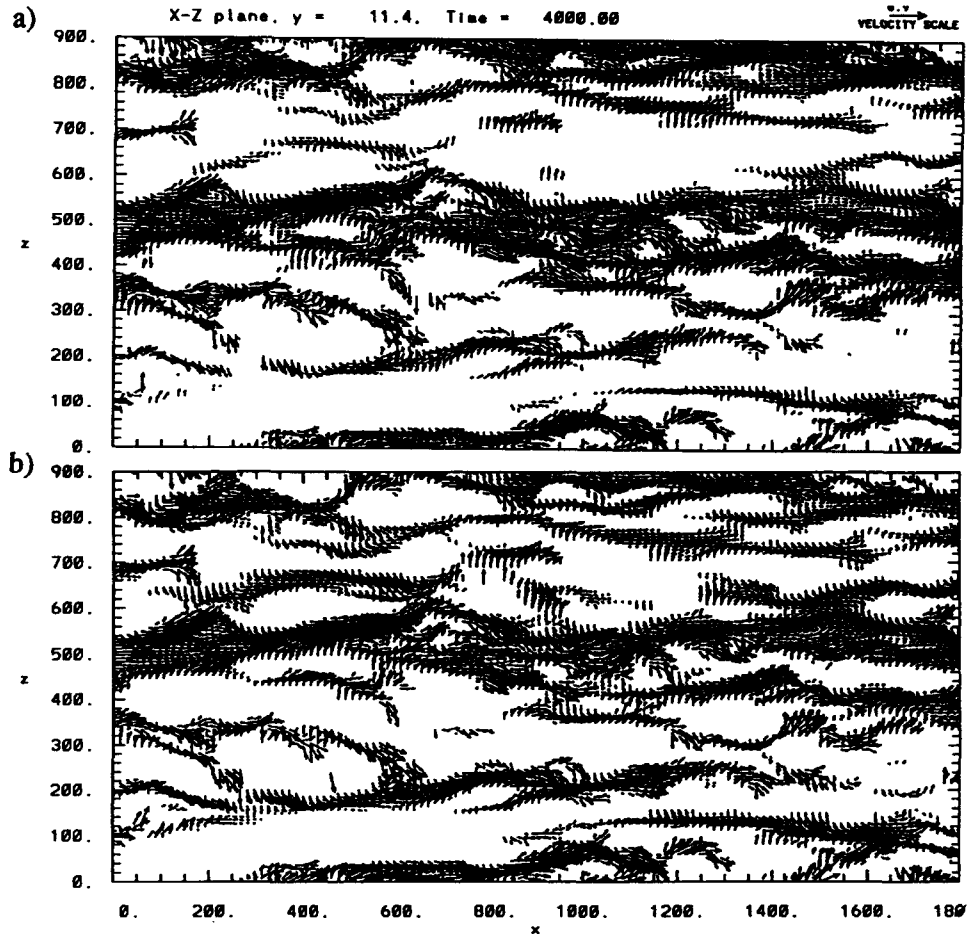

Figure 12 Instantaneous positive streamwise velocity fluctuation events in the xz-plane at $y=11.4$; a) the large structures are assumed to be part of the turbulence; b) the large structures are assumed to be part of the mean flow

where ε_{ijk} is the permutation index, and $\overline{\omega}_i$ is the ensemble average of the vorticity in the i-direction. The term on the left-hand side of Equation 11 corresponds to the convective transfer of average vorticity due to the average flow. The first term on the right side of Equation 11 gives the stretching, tilting, and twisting of the vorticity vector components in the i-direction. The second term is a source term that corresponds to vorticity generation by the turbulence. The last term represents viscous diffusion of vorticity. The components of the average vorticity vector in the present case are

$$\overline{\boldsymbol{\omega}} = (\overline{\omega}_x, \overline{\omega}_y, \overline{\omega}_z) = \left[\left(\frac{\partial w^s}{\partial y} - \frac{\partial v^s}{\partial z}\right), \frac{\partial \overline{U}_x}{\partial z}, -\frac{\partial \overline{U}x}{\partial y}\right] \tag{12}$$

The mean streamwise vorticity associated with the secondary flow is expressed as

$$\overline{\omega}_x = -\nabla^2 \psi \tag{13}$$

where ψ is defined by Equation 9.

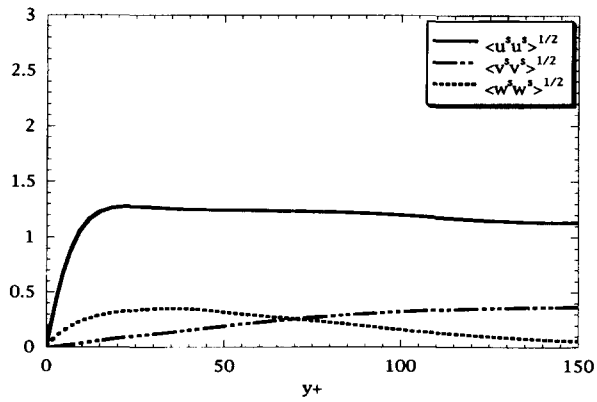

Figure 13 rms values of the secondary flow components of velocity in wall units

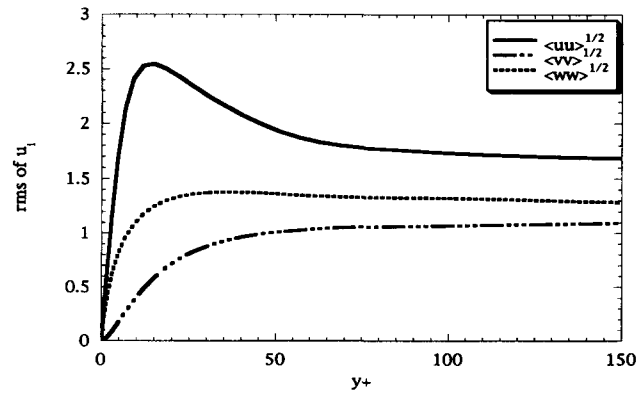

Figure 14 Turbulence intensities in wall units

Mean streamwise vorticity and streamfunction

A numerical evaluation of the terms of the momentum equation shows that the secondary flow is inviscid and not affected by turbulent stresses or viscous diffusion in the central region of the channel. The viscous terms become important only for $y < 35$. The wavy pattern of the secondary flow velocity in the spanwise direction, which was reported by Lee and Kim (1991) and confirmed in this study, along with the observation that the flow is inviscid suggests that the secondary flow pattern is rotational and described by kinematic Equation 13. Momentum Equation 6 then gives the pressure field associated with the secondary flow. Contours of x-vorticity (not presented here) confirm that the secondary flow is rotational.

From Equation 11 the transport equation for $\bar{\omega}_x$ is

$$v^s \frac{\partial \bar{\omega}_x}{\partial y} + w^s \frac{\partial \bar{\omega}_x}{\partial z} = \left(\frac{\partial^2}{\partial z^2} - \frac{\partial^2}{\partial y^2} \right) \overline{vw} + \frac{\partial^2 (\overline{v^2} - \overline{w^2})}{\partial y \, \partial z} + \frac{\partial^2 \bar{\omega}_x}{\partial y^2} + \frac{\partial^2 \bar{\omega}_x}{\partial z^2} \tag{14}$$

The secondary flow is directly related to $\bar{\omega}_x$, as is evident from Figure 9a, and the magnitude of $\bar{\omega}_x$ is a measure of the strength of the secondary flow. Terms that represent tilting of y-vorticity in the x-direction and twisting of z-vorticity in the x-direction do not appear in Equation 14, because they cancel each other. The only source terms are the turbulence terms. Speziale (1982) showed that these terms are responsible for the creation of secondary flows in noncircular ducts and developed a criterion for the appearance of secondary flows based on this argument. In the case of plane Couette flow, the turbulence terms are small. The viscous terms are important only close to the wall; they are responsible for the transfer of vorticity in and out of the field at the walls. In the core region of the channel, convection terms are dominant. They transfer $\bar{\omega}_x$ around each roll cell. Neglecting the turbulence and viscous dissipation terms, Equation 14 takes the form

$$\frac{D\bar{\omega}_x}{Dt} = 0 \tag{15}$$

for the center region of the channel. The implication of the above is that the x-vorticity associated with a fluid particle is constant in the center region of the channel; for a stationary flow, lines of constant $\bar{\omega}_x$ coincide with lines of constant ψ, because fluid particles follow the streamlines.

In the center region of the channel, the change in the value of $\bar{\omega}_x$ in the y-direction is small. Figure 16 presents values of $\bar{\omega}_x$ averaged over $y = 50 - 250$ as a function of z. The same figure shows the average value of the streamfunction ψ of the secondary flow, supporting the argument that $\bar{\omega}_x$ has the same pattern as the streamfunction.

Batchelor (1967) discussed cases for which Equation 15 holds. Because $\bar{\omega}_x$ is constant over a streamline, it can be written as a function of ψ and Equation 13 becomes

$$\bar{\omega}_x = -\left(\frac{\partial^2 \psi}{\partial y^2} + \frac{\partial^2 \psi}{\partial z^2} \right) = f(\psi) \tag{16}$$

Once $f(\psi)$ is known, a solution for the streamfunction ψ can be found. One case is a uniform vorticity in the flow (Batchelor 1956), where $f(\psi) = \omega_o = \text{const}$. The flow under consideration is

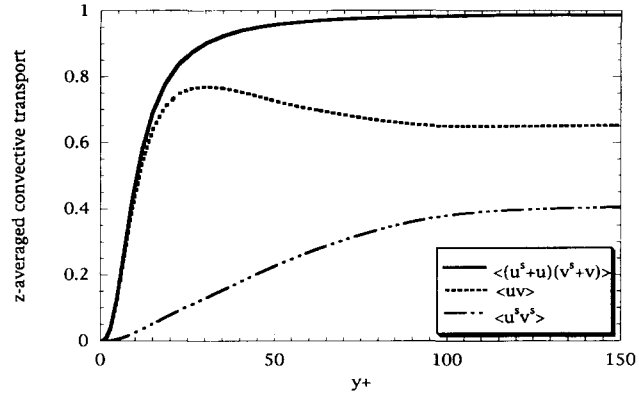

Figure 15 Relative contribution of secondary flow and turbulence to the convective transport of x-momentum in wall units

clearly not represented by a uniform $\bar{\omega}_x$. Another possibility is

$$\frac{\partial^2 \psi}{\partial y^2} + \frac{\partial^2 \psi}{\partial z^2} = -\alpha^2 \psi \tag{17}$$

This is the well-known *reduced wave equation*, the *Helmholtz equation*, or the *membrane equation*, where α is interpreted as a real wavenumber and ψ as the displacement of a vibrating elastic membrane. Equation 17 also describes the Bénard cells that result from a thermal instability (Drazin and Reid 1981). The general solution of Equation 15 is

$$\psi = C \cos(\alpha_y y) \cos(\alpha_z z) \tag{18}$$

where C is a constant, $\alpha^2 = \alpha_y^2 + \alpha_z^2$, $2\pi/\alpha_y$ is the wavelength in the y-direction and $2\pi/\alpha_z$ is the wavelength in the z-direction. Figure 17a shows the contours of the secondary flow streamfunction ψ, evaluated from the simulation data. It shows that the z-dimension of the computational box accommodates two wavelengths λ_z and the height of the channel half-wavelength λ_y in the y-direction. Thus, values of α_y and α_z can be estimated as

$$\lambda_y = 2(2h) = (4h)$$

$$\alpha_y = \frac{2\pi}{\lambda_y} = \frac{\pi}{2h} = 0.01047 \tag{19}$$

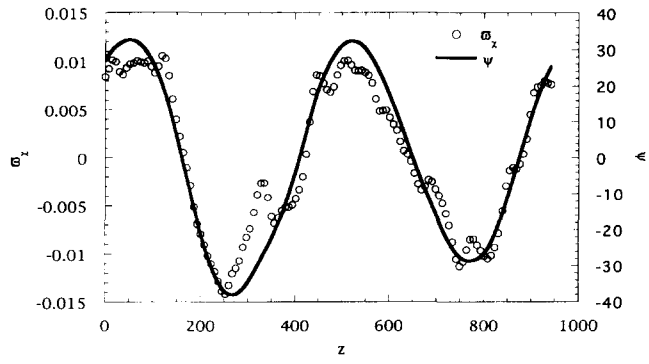

Figure 16 x-vorticity and streamfunction averaged in the center of the channel (y=50–250)

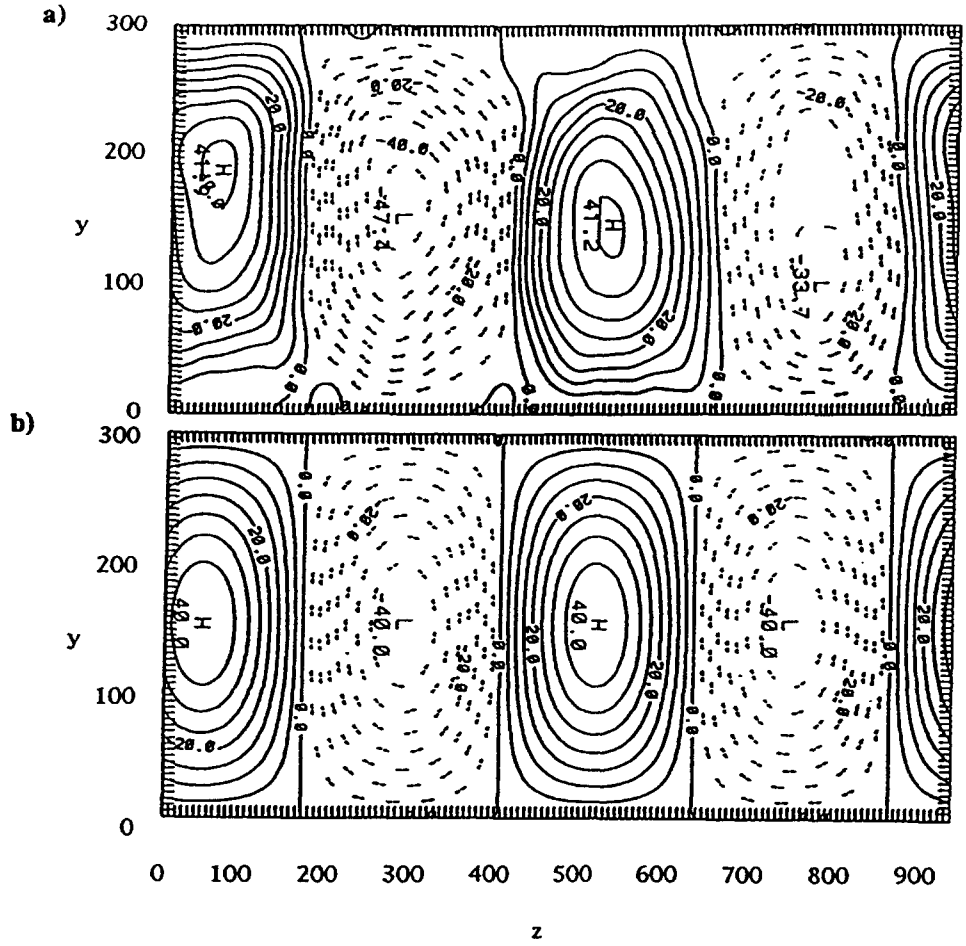

Figure 17 Contours of the streamfunction for the secondary flow; a) calculation from data; b) construction of solution

and

$$\lambda_z = \frac{2\pi h}{2} = \pi h$$

$$\alpha_z = \frac{2\pi}{\lambda_z} = \frac{2}{h} = 0.01333 \tag{20}$$

From Figure 17a, it is found that the amplitude of ψ is represented by $C \simeq 40$ and that ψ has its maximum at $z \simeq 45$. From these results and Equation 18, the following relationship is derived:

$$\psi = 40\cos(\alpha_y y)\cos[\alpha_z(z - 45)] \tag{21}$$

with α_y and α_z given by Equations 19 and 20, respectively. Figure 17b presents the construction of the streamfunction ψ using Equation 21. This is to be compared with the measurements in Figure 17a.

From Equations 16 and 17

$$\frac{\overline{\omega}_x}{\psi} = \alpha^2 \tag{22}$$

Using results at the peaks in Figure 16 a value of $\alpha^2 \simeq 0.01/32 = 3.13\ 10^{-4}$ is obtained. Using the calculated values of α_y and α_z to evaluate α, we get $\alpha^2 = \alpha_y^2 + \alpha_z^2 = 2.87\ 10^{-4}$. The two values are very close considering that the data are not perfect; averages over a much larger time span might be necessary in order to see perfect roll cells.

Equation 21 is a good representation of the secondary flow in the core region of the channel, where the assumption of inviscid flow holds. There is a boundary layer close to the wall, where viscosity effects are significant. Figure 18 presents w^s averaged over half of a roll cell. At the center of the channel, w^s is zero. As the distance from the center of the roll cell increases the magnitude of w^s also increases until it reaches a maximum at $y \simeq 35$. Close to the wall w^s decreases rapidly toward zero on the

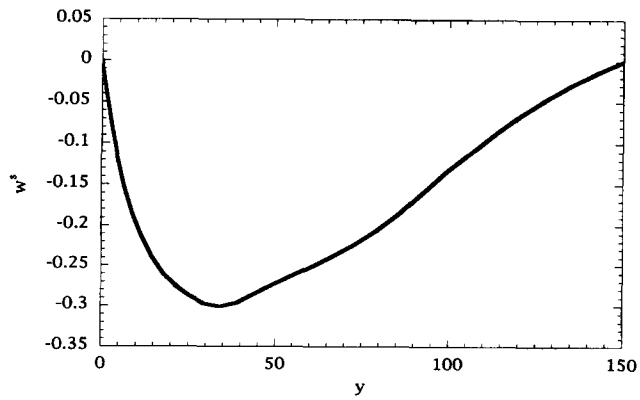

Figure 18 w^s averaged over half roll-cell

wall. Furthermore, it is found that $\bar{\omega}_x$ changes sign at $y \simeq 35$ indicating the existence of a viscous region for $y < 35$.

Kinetic energy equation for secondary flow

An important issue is how the secondary flow is sustained. The kinetic energy equation for the secondary flow needs to be considered. From Equations 10 and 5, the y-component of the secondary flow kinetic energy is defined by

$$\frac{1}{2}\left(\frac{\partial v^{s^2} v^s}{\partial y} + \frac{\partial v^{s^2} w^s}{\partial z}\right) + \frac{\partial v^s \overline{v^2}}{\partial y} + \frac{\partial u^s \overline{vw}}{\partial z} - \overline{v^2}\frac{\partial v^s}{\partial z} - \overline{vw}\frac{\partial v^s}{\partial z}$$

$$= -v^s \frac{\partial p^s}{\partial y} + 2\frac{\partial}{\partial y}\left(v^s \frac{\partial v^s}{\partial y}\right) + \frac{\partial}{\partial z}\left[v^s\left(\frac{\partial v^s}{\partial z} + \frac{\partial w^s}{\partial y}\right)\right]$$

$$-2\left(\frac{\partial v^s}{\partial y}\right)^2 - \frac{\partial v^s}{\partial z}\left(\frac{\partial v^s}{\partial z} + \frac{\partial w^s}{\partial y}\right) \qquad (23)$$

and the z-component, by

$$\frac{1}{2}\left(\frac{\partial w^{s^2} v^s}{\partial y} + \frac{\partial w^{s^2} w^s}{\partial z}\right) + \frac{\partial w^s \overline{vw}}{\partial y} + \frac{\partial w^s \overline{w^2}}{\partial z} - \overline{vw}\frac{\partial w^s}{\partial y} - \overline{w^2}\frac{\partial w^s}{\partial z}$$

$$= -w^s \frac{\partial p^s}{\partial z} + \frac{\partial}{\partial y}\left[w^s\left(\frac{\partial w^s}{\partial y} + \frac{\partial w^s}{\partial z}\right)\right] + 2\frac{\partial}{\partial z}\left(\frac{\partial w^s}{\partial z}\right)$$

$$-\frac{\partial w^s}{\partial y}\left(\frac{\partial w^s}{\partial y} + \frac{\partial v^s}{\partial z}\right) - 2\left(\frac{\partial w^s}{\partial z}\right)^2 \qquad (24)$$

where p^s is used instead of $\bar{P}$ to denote the ensemble average of the pressure, which is associated with the secondary flow. It is noted that because of the assumption of homogeneity in the flow direction, the streamwise velocities $\langle U \rangle$ and u^s do not appear in Equations 21 and 22.

The first four terms in each equation represent the transport of secondary flow kinetic energy by the secondary flow and by the fluctuations. They are terms that convect energy around the field without consuming or producing it. The last two terms on the left-hand sides are sources or sinks. They transfer energy between the secondary motion and the turbulence and are the only possible sources of energy. Thus, these equations suggest that the net contribution from these terms must be positive for a stationary secondary flow to exist. The pressure terms redistribute energy between the y- and z-components. Work done by the viscous stresses acting on the secondary flow is represented by the next two terms. The last two terms represent the viscous dissipation of the secondary flow kinetic energy. Because the convection and diffusion terms conserve kinetic energy and the dissipation consumes it, the terms that represent the supply of energy to the secondary flow are associated with the interchange of energy between fluctuations and the secondary motion. Thus, the energy balance equation suggests that a secondary flow can be sustained if the dissipation of the secondary flow by viscosity is balanced by energy supplied to the secondary flow by turbulence.

Figure 19 presents these terms averaged over z; $\overline{ww}(\partial w^s/\partial z)$ and $\overline{vw}(\partial w^s/\partial y)$ have positive values close to the wall, change sign farther away and finally go to zero at the center of the channel, which is expected, because w^s is zero there. On the other hand, $\overline{vv}(\partial v^s/\partial y)$ is negative close to the wall and approaches zero at the center of the channel, while $\overline{vw}(\partial v^s/\partial_z)$ is positive throughout the channel. Equations 23 and 24 show that a positive sign for these terms means that they are sources of kinetic energy (because they behave opposite to dissipation), and a negative sign means that they are sinks of kinetic energy. Thus, $\overline{vv}(\partial v^s/\partial y)$ extracts energy from the secondary velocity gradient and feeds it to the turbulence and $\overline{vw}(\partial v^s/\partial z)$ transfers energy from the turbulence to the secondary flow. The integrals of the different terms, presented in Figure 19, over the whole extent of the channel (twice that shown) give the values shown. The net effect is a supply of kinetic energy to the secondary motion. Term $\overline{vw}(dv^s/dz)$ is seen to be the major factor in transferring energy from the turbulence to the secondary flow.

Figure 20a presents a quadrant analysis of $\overline{vw}(\partial v^s/\partial z)$ at $y = 73$, where the maximum occurs. The points in the figure form a cloud around a 45° line through quadrants three and one, indicating that, most of the time, $\partial v^s/\partial_z$ and $\overline{vw}$ are either both negative or both positive. The same behavior is exhibited by $\partial w^s/\partial y$ and $\overline{vw}$ in the region close to the wall, as is shown in Figure 20c. Figures 20a and 20c are the opposite of what is usually found for the relation between Reynolds stresses and corresponding average velocity gradients. Figure 20b presents a quadrant analysis of $\overline{vw}(\partial w^s/\partial y)$ at $y = 50$. The cloud of points mostly occupies quadrants two and four; where $\partial w^s/\partial y$ and $\overline{vw}$ have opposite signs.

An eddy-viscosity ε associated with $\overline{vw}$ can be defined as $-\overline{vw} = 2\varepsilon D_{23}$. Multiplication of both sides of this relation by D_{23} gives

$$-\overline{vw}\left(\frac{\partial v^s}{\partial z} + \frac{\partial w^s}{\partial y}\right) = \varepsilon\left(\frac{\partial v^s}{\partial z} + \frac{\partial w^s}{\partial y}\right)^2 \qquad (25)$$

where the left-hand side is the sum of two terms, discussed above and presented in Figure 19. It follows from Equation 25 that when $\overline{vw}(\partial v^s/\partial z + \partial w^s/\partial y)$ is positive on average, as is found to be the case for $y < 35$, the eddy-viscosity is negative. Similarly, the eddy-viscosity associated with $\overline{ww}$ is negative for $y < 40$. These results suggest that, in (3-D) mean flows, the use of Newtonian concepts to represent turbulent stresses requires the recognition that stresses are related to all components of the rate of strain tensor (Hinze 1987). Thus, $-\overline{vw} = f(D_{23}, D_{22}, D_{33})$ and not just of D_{23}, as would be the case for an isotropic medium.

The mechanism governing the transfer kinetic energy from the fluctuations to the secondary flow is, therefore, different from what is usually found in flows that are approximately unidirectional. The common situation is that, on average, kinetic energy is extracted from the mean flow by the turbulence through the Reynolds stresses. In the present case, the secondary motion

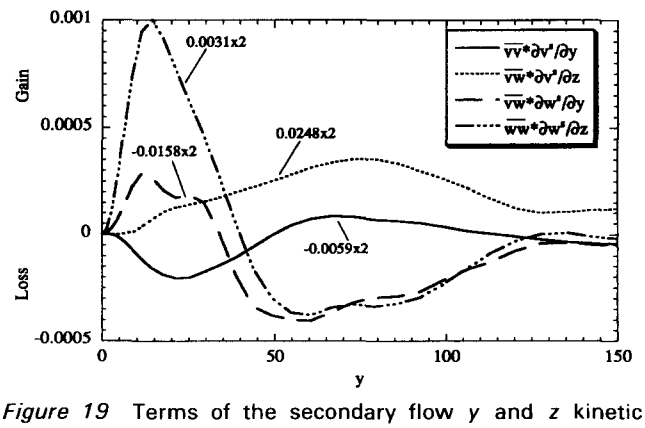

Figure 19 Terms of the secondary flow y and z kinetic energy equations, which show the interchange of kinetic energy between fluctuations and secondary motion, averaged over z

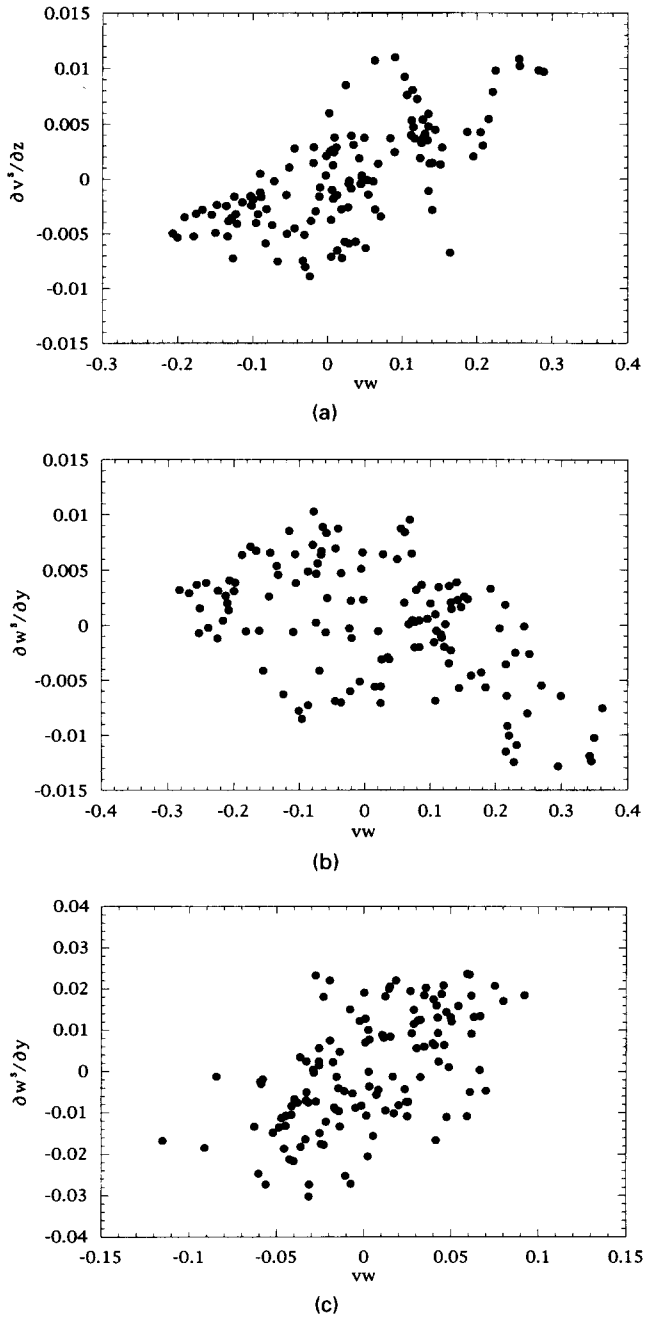

Figure 20 Quadrant analysis of source/sink terms of the secondary flow kinetic energy equations; a) quadrant analysis of $\overline{vw}(\partial v^s/\partial z)$ at the location of its maximum; b) quadrant analysis of $\overline{vw}(\partial w_s/\partial y)$ at the location of its minimum; c) quadrant analysis of $\overline{vw}(\partial w^s/\partial y)$ at the location of its maximum

affects the turbulence and modulates the Reynolds stresses in a way that they can cause a supply of energy to the secondary flow. Thus, small scales of motion supply kinetic energy to larger scales, contrary to the usual notions of an energy cascade.

The net kinetic energy supplied to the secondary flow in one unit of time is calculated to be less than 0.001 of the total secondary flow kinetic energy; it is balanced by the viscous dissipation close to the walls ($y < 15$), mainly through $(\partial w^s/\partial y)^2$. Once the roll cells are established, it seems that a very small amount of energy is needed to sustain them.

Kinetic energy equation for the streamwise velocity

The spanwise average of the streamwise kinetic energy defined by Equation 8 has two terms, because

$$\langle \overline{U}^2 \rangle = \langle U \rangle^2 + \langle u^{s2} \rangle \tag{26}$$

Separate equations for $\langle U \rangle^2$ and u^{s2} are obtained by using the statistical theorem that the average of a sum is the sum of the averages and by applying the Reynolds averaging assumption to the secondary flow:

$$\left\langle \frac{\partial *}{\partial x_j} \right\rangle = \frac{\partial \langle * \rangle}{\partial x_j} \tag{27}$$

Equation 27 has been justified empirically. For example, zero values of $\langle \partial u^s/\partial y \rangle$, $\langle \partial v^s/\partial y \rangle$, $\langle \partial w^s/\partial y \rangle$ are obtained from the computer simulation for all values of y.

The following equation is then derived from Equation 4:

$$\langle U_j \rangle \frac{\partial \langle U_i \rangle}{\partial x_j} = \frac{\partial^2 \langle U_i \rangle}{\partial x_j^2} - \frac{\partial \langle \overline{u_i u_j} \rangle}{\partial x_j} - \frac{\partial \langle \overline{u_i^s u_j^s} \rangle}{\partial x_j} \tag{28}$$

A kinetic energy equation for $\langle U_i \rangle$ is obtained by multiplying Equation 26 by $\langle U_i \rangle$. The streamwise component of this equation gives

$$\frac{d\langle U \rangle \langle u^s v^s \rangle}{dy} + \frac{d\langle U \rangle \langle \overline{uv} \rangle}{dy} - \langle u^s v^s \rangle \frac{d\langle U \rangle}{dy} - \langle \overline{uv} \rangle \frac{d\langle U \rangle}{dy}$$

$$= \frac{d}{dy}\left(\langle U \rangle \frac{d\langle U \rangle}{dy} \right) - \left(\frac{d\langle U \rangle}{dy} \right)^2 \tag{29}$$

A spanwise averaged kinetic energy equation for u_i^s is obtained by subtracting the kinetic energy equation for $\langle U_i \rangle$ from the spanwise average of Equation 8. The streamwise component of this equation gives

$$\langle u^s v^s \rangle \frac{d\langle U \rangle}{dy} + \frac{1}{2} \frac{d\langle u^{s2} \rangle v^s}{dy} + \frac{d\langle u^s \overline{uv} \rangle}{dy}$$

$$- \left\langle \overline{uv} \frac{\partial u^s}{\partial y} \right\rangle - \left\langle \overline{uw} \frac{\partial u^s}{\partial z} \right\rangle$$

$$= \frac{d}{dy}\left\langle u^s \frac{\partial u^s}{\partial y} \right\rangle - \left\langle \left(\frac{\partial u^s}{\partial y} \right)^2 \right\rangle - \left\langle \left(\frac{\partial u^s}{\partial z} \right)^2 \right\rangle \tag{30}$$

The term $\langle u^s v^s \rangle (d\langle U \rangle/dy)$ appearing both in Equations 27 and in 28 is a sink for $\langle U \rangle$ kinetic energy and source for u^s kinetic energy. There is, thus, a transfer of energy from $\langle U \rangle$ to u^s. Term $\langle \overline{uv} \rangle (d\langle U \rangle/dy)$ in Equation 29 is a sink that represents a transfer of $\langle U \rangle$ energy to the u-turbulence. Energy from u^s is transferred to u-turbulence, through the terms $\langle \overline{uv}(\partial u^s/\partial y) \rangle$ and $\langle \overline{uw}(\partial u^s/\partial z) \rangle$. The modification of the Reynolds stresses by the secondary flow allows a transfer of energy from the turbulence to v^s and w^s energy. Thus, Equation 29 shows that energy transferred to the flow field through the work done by moving the walls (which is obtained by integrating the term $(d/dy)(\langle U \rangle (d\langle U \rangle/dy))$ over the y-domain) does not go directly to the secondary flow, but takes the indirect path pictured in

Figure 21. Here, the first line represents the net effect of Equation 27 and the second line, the net effect of Equation 28. What is not indicated in this pictorial representation is the feedback whereby v^s and w^s result in the production of u^s energy and the modification of v-turbulence and w-turbulence so as to produce nonzero values of $\overline{vw}$, and $\overline{uw}$ and variations of $\overline{u^2}, \overline{v^2}, \overline{w^2}$ in the z-direction. These modifications allow a transfer of energy from the v-turbulence and w-turbulence to the secondary flow, as indicated in Figure 21.

Conclusions and discussion

Interpretation of the large-flow structures

Computational studies of turbulent Couette flow have revealed a strongly streaky structure (Figure 8a) in the streamwise velocity component in the core region that is not observed in a turbulent Poiseuille flow. This finding has been confirmed in studies conducted with different initial conditions, different lengths of the computational domain, and different numerical methods. Lee and Kim (1991) used a box which was 2135^+ long, 340^+ high, and 1425^+ wide and discovered contributions to the kinetic energy and to the Reynolds stress by roll cells extending over the whole length of the box ($k_x = 0$ mode). Papavassiliou (1993) confirmed these results and showed that the roll cells do not change significantly for times as large as 2000^+ units or about one turnover time (in a box that is 1900^+ long, 300^+ high, and 950^+ wide).

It is expected that these streaks would be observed to meander if a large enough box were used. Nevertheless, they are persistent enough in space and in time that it is attractive to consider them as associated with eddy structures that may be approximated as secondary flows in order to provide an interpretation. The spanwise and normal velocities of this secondary flow are small. However, because of their persistence, they can make significant contributions to the transport of momentum and can produce organized spanwise variations of the streamwise velocity (observed as a streaky structure).

Calculations of the terms in the momentum equations describing the secondary flow reveal that the viscous and turbulent stresses are important for $y < 35$. In the core region, the secondary flow is rotational and inviscid, so that lines of constant vorticity coincide with the streamlines. It is shown that the streamfunction of the secondary motion in the core of the channel is described by the reduced wave equation and a solution of this equation, which agrees well with the calculated values of the streamfunction has been found. The walls of the channel create a boundary layer for the spanwise average velocity. Here, viscous effects cannot be ignored.

Couette flow differs from Poiseuille flow in that the velocity profile is asymmetric. In the Couette system, considered in this paper, flows outward from the bottom wall that extract energy from the mean flow (a quadrant one event), continue to do so when they move past the center line of the channel. The opposite is true for turbulent Poiseuille flow. Consequently, conditions are favorable for the enhancement of turbulent structures that extend from wall to wall.

For these structures to develop into roll cells, they must affect the turbulence in a special way. The secondary flow introduces new Reynolds stresses and creates a nonhomogeneous field in the spanwise direction. The computations show that Reynolds stresses defined with reference to the 3-D flow are associated with a net transfer of energy to the secondary flow. This is an example of Prandtl's second kind of secondary flow (Bradshaw 1987), a stress-induced pattern.

Conditions for existence

Results presently available suggest that the existence and the properties of the large-flow structures could depend on the Reynolds number and the box dimensions. The total energy of the secondary flow is obtained by adding the z-averaged Equa-

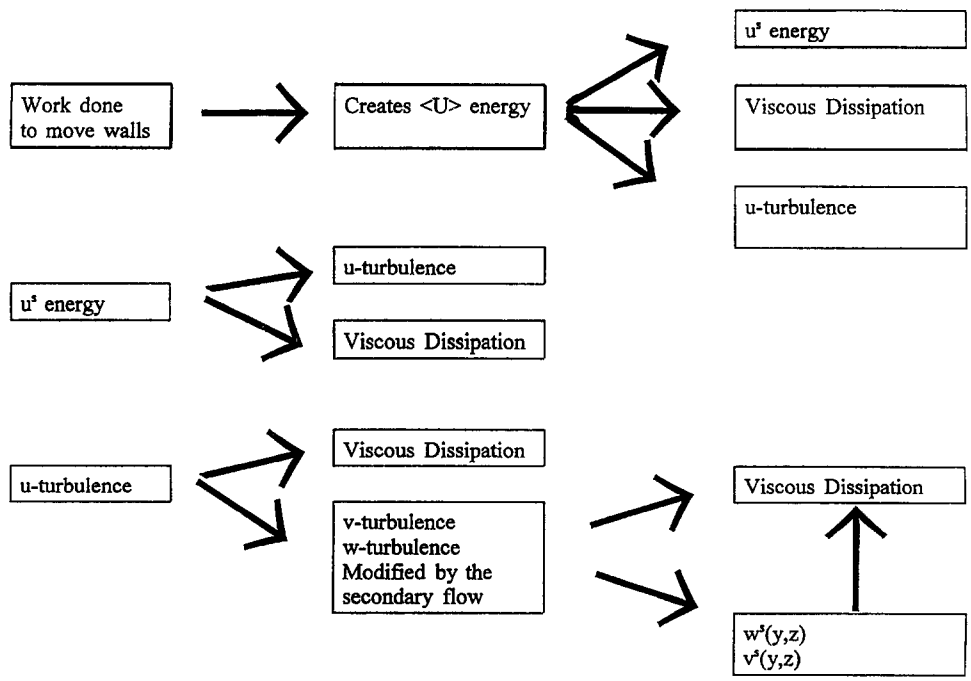

Figure 21 Sequence of kinetic energy transfer events

tions 23 and 24 to Equation 30

$$\frac{1}{2}\frac{\partial\langle u_i^{s2}u_i^s\rangle}{\partial x_j}+\frac{\partial\langle u_i^s\overline{u_iu_j}\rangle}{\partial x_j}-\left\langle\overline{u_iu_j}\frac{\partial u_i^s}{\partial x_j}\right\rangle+\langle u_i^su_j^s\rangle\frac{\partial\langle U_i\rangle}{\partial x_j}$$
$$=-\left\langle u_i^s\frac{\partial p^s}{\partial x_i}\right\rangle+\left\langle\frac{\partial}{\partial x_j}u_i^s\left(\frac{\partial u_i^s}{\partial x_j}+\frac{\partial u_j^s}{\partial x_i}\right)\right\rangle$$
$$-\left\langle\frac{\partial u_i^s}{\partial x_j}\left(\frac{\partial u_i^s}{\partial x_j}+\frac{\partial u_j^s}{\partial x_i}\right)\right\rangle \qquad (31)$$

The Reynolds number enters through the boundary conditions, the specification of $\langle U\rangle$, and the turbulence properties. We could expect that there is a minimum Reynolds number for which Equation 31 can be satisfied. Furthermore, the properties of the secondary flow should be defined by a consideration of Equations 23, 24, 30, and 31. This will require an understanding of Reynolds stresses in a 3-D flow.

More general implications

The results presented in this paper could have more general implications in considering turbulent flows. Firstly, Figures 11 and 12 show that the properties of the wall vortices depend on outer flow structures that scale with the dimensions of the system. This, then, raises concerns as to whether all aspects of the near-wall flow will scale with the wall parameters, friction velocity, and kinematic viscosity.

The mechanism of energy transfer used to interpret the large-scale structures implies that a reverse energy cascade is possible in turbulent flows. Even if the secondary flow structures observed in this study would meander in a much wider and a much longer flow field, the finding that kinetic energy is supplied to larger scales of motion by smaller eddies will be important in understanding their behavior. Questions that remain unanswered are the following: What are the conditions for the existence of these secondary flows? What governs their properties? and What starts them?

Acknowledgments

This work is being supported by the National Science Foundation through grant CTS-92-00936. We also acknowledge the support and facilities of the National Center for Supercomputing Applications at the University of Illinois in Urbana, Illinois.

References

Aydin, M. and Leutheusser, H. J. 1979. Novel experimental facility for the study of plane Couette flow. *Rev. Sci. Instrum.*, **50**, 1362–1366

Aydin, M. and Leutheusser, H. J. 1991. Plane-Couette flow between smooth and rough walls. *Exp. Fluids*, **11**, 302–312

Batchelor, G. K. 1967. *An Introduction to Fluid Dynamics*. Cambridge University Press, New York, chapter 7

Batchelor, G. K. 1956. On steady laminar flow with closed streamlines at large Reynolds numbers. *J. Fluid Mech.*, **1**, 177–194

Bech, K. H. and Andersson, H. I. 1994. Very large-scale structures in DNS. In *Direct and Large Eddy Simulation I*, P. R. Voke (ed.), Kluwer, The Netherlands

Bech, K. H., Andersson, H. I. and Kristoffersen, R. 1993. Inner layer velocity statistics in plane Couette flow. In *Near-Wall Turbulent Flows*, R. M. C. So, C. G. Spezialle and B. E. Launder (eds.), Elsevier Science, New York

Bech, K. H., Tillmark, N., Alfredsson, P. H. and Andersson, H. I. 1995. An investigation of turbulent plane Couette flow at low Reynolds numbers. *J. Fluid Mech.*, **286**, 291–325

Bradshaw, P. 1987. Turbulent secondary flows. *Ann. Rev. Fluid Mech.*, **19**, 53–74

Chandrashekhar, S. 1961. *Hydrodynamic and Hydromagnetic Stability*. Oxford University Press, New York, 272–342

Drazin, P. G. and Reid, W. H. 1981. *Hydrodynamic Stability*. Cambridge University Press, New York, 82–83, 256–263

El Telbany, M. M. M. and Reynolds, A. J. 1980. Velocity distribution in plane turbulent channel flows. *J. Fluid Mech.*, **100**, 1–29

El Telbany, M. M. M. and Reynolds, A. J. 1982. The structure of turbulent plane Couette flow. *J. Fluids Eng.*, **104**, 367–372

Hinze, J. O. 1987. *Turbulence*. 2nd ed., McGraw-Hill, New York, 15–29

von Kármán, Th. 1937. The fundamentals of the statistical theory of turbulence. *J. Aeron. Sci.*, **4**, 131–138

Komminaho, J., Lundbladh, A. and Johansson, A. V. 1996. Very large structures in plane turbulent Couette flow. *J. Fluid Mech.*, to appear

Lee, M. J. and Kim, J. 1991. The structure of turbulence in a simulated plane Couette flow. *Proc. 8th Symposium on Turbulent Shear Flows* (Paper 5-3), Munich

Leutheusser, H. J. and Chu, V. H. 1971. Experiments on plane Couette flow. *Proc. ASCE, H. Hydr. Div.*, **97**, 1269–1284

Lundbladh, A. and Johansson, A. V. 1991. Direct simulation of turbulent spots in plane Couette flow. *J. Fluid Mech.*, **229**, 499–516

Lyons, S. L. 1989. Ph.D. thesis, University of Illinois, Urbana, IL

Lyons, S. L., Hanratty, T. J. and McLaughlin, J. B. 1991. Large-scale computer simulation of fully developed turbulent channel flow with heat transfer. *Numer. Methods Fluids*, **13**, 999–1028

Marcus, P. S. 1984. Simulation of Taylor-Couette flow. *J. Fluid Mech.*, **146**, 45–64

Miyake, Y., Kajishima, T. and Obana, S. 1987. Direct numerical simulation of plane Couette flow at transitional Reynolds number. *JSME Int. J.*, **30**, 57–65

Monin, A. S. and Yaglom, A. M. 1971. *Statistical Fluid Mechanics: Mechanics of Turbulence*. Vol. 1, MIT Press, Cambridge, MA

Niederschulte, M. A. 1989. Ph.D. thesis, University of Illinois, Urbana, IL

Orszag, S. A. and Kells, L. C. 1980. Transition to turbulence in plane Poiseuille and plane Couette flow. *J. Fluid Mech.*, **96**, 159–205

Papavassiliou, D. V. 1993. M.S. thesis, University of Illinois, Urbana, IL

Reichardt, H. 1956. Uber die Geschwindigkeitsveteilung in einer deradlinigen turbulenten Couettesströmung. *Z. AMM*, **36**, Sonderheft, 26–29

Robertson, J. M. 1959. On turbulent plane-Couette flow. *Proc. 6th Midwestern Conference Fluid Mech.*, University of Texas, Austin, TX, 169–182

Robertson, J. M. and Johnson, H. F. 1970. Turbulence structure in plane Couette flow. *Proc. ASCE J. Eng. Mech. Div.*, **96**, (EM6), 1171–1182

Speciale, C. G. 1982. On turbulent secondary flows in pipes of noncircular cross-section. *Int. J. Eng. Sci.*, **20**, 863–867

Tillmark, N. and Alfredsson, P. H. 1992. Experiments on transition in plane Couette flow. *J. Fluid Mech.*, **235**, 89–102